Electronic Supplementary Material (ESI) for Physical Chemistry Chemical Physics.
This journal is © the Owner Societies 2019

Electronic Supplementary Information

Structural manifestation of partial proton ordering and defect mobility in ice I*h*

A. Dominic Fortes,[1,2,*]

[1] ISIS Neutron & Muon Spallation Source, Rutherford Appleton Laboratory, Harwell Science and Innovation Campus, Chilton, Oxfordshire, OX11 0QX, United Kingdom.
[2] Department of Earth Sciences, University College London, Gower Street, London WC1E 6BT, United Kingdom.

*Corresponding author email: dominic.fortes@stfc.ac.uk

Contents

Section S1: Further experimental methodology – list of measurement series

Three separately-prepared samples of D_2O ice I*h* were studied over a nine-day period at the end of June 2018, subdivided below into a series of different thermal protocols comprising measurements at 201 discrete temperature points (Series 1 – 5 detailed below).

The raw data is archived at doi:10.5286/ISIS.E.95699847.

A single sample of KOD-doped ice I*h* was studied over a three-day period at the end of September 2018, again with a series of applied thermal protocols, comprising 86 discrete temperature points (Series 6 & 7 detailed below).

The raw data is archived at doi:10.5286/ISIS.E.98018903.

The refined lattice parameters, derived *c*/*a* ratios and the derived linear and volume thermal expansion coefficients are tabulated in the Supplementary Data Tables S1 and S2.

Series 1 (naturally-frozen ice, slowly cooled then slowly warmed)

The sample was mounted in the CCR at ~ 80 K and warmed over the space of ~ 1 hr to 240 K. Data were collected in 10 K increments on cooling to 10 K, counting for ~ 13 minutes of real time (10 μA of integrated proton current). Data were collected for 1 hr (40 μA) at 10 K. Measurements were then made on warming from 15 to 265 K in 10 K increments, interleaved with the slow-cool measurements, counting each for 10 μA.

Series 2 (LN_2-quench / warm / re-cool)

After the measurement at 265 K was completed, the sample stick was removed from the cryostat and the sample holder was directly immersed in liquid nitrogen. Cooling of the Al-alloy cell was observed to occur at a rate of −170 K min^{-1}, after which the sample was left immersed in LN_2 for ~ 1 hr whilst the CCR temperature was brought down to 80 K. The sample stick was then re-inserted and cooled to 10 K over the course of another hour. From 10 K the sample was warmed in 10 K increments to 250 K and then re-cooled in 10 K increments back down to 100 K, 20 K increments from 80 – 20 K with a final measurement at 10 K.

Series 3 (Fast cool from 170 K / warm)

From 10 K, the sample was warmed at 3 K min^{-1} to 170 K whilst maintaining the background temperature of the CCR cold-head as low as possible. The sample was maintained at 170 K for 20 minutes before the heater power was cut and the cell was permitted to cool at the fastest achievable rate (15 K min^{-1}).

Data were then collected on warming in 5 K increments from 10 to 160 K and 10 K increments from 170 – 270 K.

Series 4 (Flash-frozen globule of D_2O)

The Series 1 – 3 specimen was extracted from the sample holder under liquid nitrogen, transferred to a sealed glass bottle and allowed to melt. Three days later, this liquid D_2O

sample was poured directly into a pool of liquid nitrogen to form a single polycrystalline lump. This lump of ice was ground to a powder and transferred to the same sample holder (incl. the same sensor and heater cartridge) as was used for Series 1 – 3. This sample was inserted into the CCR at 80 K and cooled to 10 K. Following a 1 hr data collection at 10 K, further measurements were made on warming; 10 K increments were used at low and high temperatures, but 5 K increments were used in the region between 70 and 160 K.

Series 5 (Flash frozen pipette droplet)

Finally, a fresh batch of 99.96 atom % D_2O was flash frozen by pipetting droplets into liquid nitrogen, as was done in my previous experimental study. Again, this was powdered and loaded into a sample container under liquid nitrogen. The sample holder (incl. sensor and heater) was the same one used for Series 1 – 4 above. The same thermal protocol as the previous warming runs was employed; cool quickly to 10 K, count for one hour and then warm in 10 K increments to 260 K counting for 10 μA (13 minutes) at each point.

Series 6 (KOD-doped ice, slow warm with annealing at 70 K)

The sample was loaded into the cryostat at 200 K and cooled to 1.8 K over a period of 2 hr, after which data were collected for 40 μA (1 hr). Measurements were then made in 5 K increments up to 70 K, counting each for 15 μA (21 minutes). After annealing at 70 K for 15 hr, further measurements were made on warming in 10 K increments to 270 K with counting times of 10 μA.

Series 7 (KOD-doped ice, slow cool / warm)

Upon completion of the 270 K measurement in Series 6 the sample was cooled slowly, measuring in 5 K increments to 5 K, counting for 10 μA at each point. The sample was then re-warmed to 240 K, measuring in 10 K increments for 10 μA at each datum.

Section S2: Supplementary Data Tables

Table S1: Refined lattice parameters and axial ratios of D_2O ice I*h* as a function of temperature. The temperatures shown are the average of all logged data acquired during the measurement and the stated uncertainty is the standard deviation of those values. It will be observed that the standard deviations are a few times larger amongst many of the low-temperature measurements, probably because the control-PIDs are slightly sub-optimally tuned in this region. The uncertainties on the lattice parameters are those reported by *GSAS* and the uncertainties on the *c*/*a* ratio are propagated directly from the lattice parameter uncertainties. Note that the error bars in all of the figures report twice this value since the scatter of the observations suggests that this is a better indication of the true systematic error.

Series 1 (Naturally-frozen ice slow-cooled from 240 K)			
T (K)	*a*-axis (Å)	*c*-axis (Å)	*c*/*a* ratio
240.00(1)	4.519569(9)	7.359517(24)	1.628367(6)
230.00(1)	4.517231(14)	7.355797(38)	1.628386(10)
219.99(1)	4.515013(13)	7.352293(37)	1.628410(9)
210.00(1)	4.512899(12)	7.348834(33)	1.628406(8)
200.00(1)	4.510911(12)	7.345634(31)	1.628415(8)
189.99(1)	4.509071(11)	7.342545(31)	1.628394(8)
180.00(1)	4.507319(11)	7.339726(30)	1.628402(8)
169.99(1)	4.505693(11)	7.337012(31)	1.628387(8)
160.00(1)	4.504211(11)	7.334430(29)	1.628350(8)
150.00(1)	4.502830(11)	7.332175(29)	1.628348(8)
140.00(1)	4.501579(10)	7.330042(28)	1.628327(7)
130.00(1)	4.500515(10)	7.328099(27)	1.628280(7)
120.00(1)	4.499597(10)	7.326304(27)	1.628213(7)
109.99(1)	4.498757(10)	7.324879(26)	1.628201(7)
100.00(1)	4.498092(10)	7.323740(26)	1.628188(7)
89.99(1)	4.497567(10)	7.322899(25)	1.628191(7)
79.99(1)	4.497190(9)	7.322323(24)	1.628200(6)
70.00(2)	4.496980(9)	7.322012(23)	1.628206(6)
59.99(3)	4.496901(9)	7.321966(23)	1.628225(6)
50.01(2)	4.496947(9)	7.322047(23)	1.628226(6)
39.99(4)	4.497099(9)	7.322254(23)	1.628217(6)
30.01(2)	4.497291(9)	7.322698(22)	1.628246(6)
19.99(2)	4.497473(9)	7.322980(22)	1.628243(6)
9.99(2)	4.497548(6)	7.323092(16)	1.628241(4)
15.01(2)	4.497524(9)	7.323030(22)	1.628236(6)
25.00(3)	4.497388(8)	7.322788(22)	1.628231(6)
35.01(3)	4.497185(9)	7.322492(24)	1.628239(6)
45.01(4)	4.497008(9)	7.322180(23)	1.628234(6)

55.01(2)	4.496907(9)	7.321968(22)	1.628223(6)
65.01(2)	4.496912(9)	7.321932(23)	1.628213(6)
75.00(1)	4.497061(9)	7.322147(23)	1.628207(6)
85.00(1)	4.497354(9)	7.322573(24)	1.628196(6)
95.00(0)	4.497818(9)	7.323287(24)	1.628187(6)
105.00(1)	4.498425(9)	7.324245(25)	1.628180(6)
115.00(1)	4.499174(10)	7.325503(25)	1.628188(7)
125.01(1)	4.500038(10)	7.327145(27)	1.628241(7)
135.01(1)	4.501057(10)	7.329016(27)	1.628288(7)
145.00(1)	4.502221(11)	7.331111(29)	1.628332(8)
155.00(1)	4.503505(10)	7.333273(28)	1.628348(7)
165.01(1)	4.504921(11)	7.335716(31)	1.628378(8)
175.00(0)	4.506480(11)	7.338353(29)	1.628400(8)
185.01(1)	4.508175(12)	7.341096(32)	1.628396(8)
195.01(1)	4.509980(11)	7.344066(31)	1.628403(8)
205.00(1)	4.511921(12)	7.347162(31)	1.628389(8)
215.01(1)	4.513956(12)	7.350488(34)	1.628392(9)
225.01(1)	4.516099(12)	7.353963(34)	1.628388(9)
235.00(1)	4.518356(13)	7.357586(37)	1.628377(9)
245.00(1)	4.520746(13)	7.361402(37)	1.628360(9)
255.00(1)	4.523211(13)	7.365370(39)	1.628350(10)
265.01(1)	4.525831(12)	7.369477(35)	1.628315(9)

Series 2 (Naturally-frozen ice quenched from 265 to 77 K)

T (K)	*a*-axis (Å)	*c*-axis (Å)	*c*/*a* ratio
9.99(12)	4.497611(7)	7.323696(18)	1.628352(5)
20.00(2)	4.497493(9)	7.323450(23)	1.628340(6)
30.01(4)	4.497315(9)	7.323162(23)	1.628341(6)
39.99(3)	4.497110(9)	7.322818(25)	1.628339(6)
50.00(3)	4.496964(9)	7.322565(25)	1.628335(6)
59.99(3)	4.496912(9)	7.322409(25)	1.628319(6)
70.01(2)	4.496977(9)	7.322588(26)	1.628336(7)
80.00(3)	4.497199(9)	7.322926(25)	1.628330(6)
90.00(0)	4.497561(9)	7.323521(25)	1.628332(6)
100.00(1)	4.498103(10)	7.324309(27)	1.628311(7)
110.00(1)	4.498829(10)	7.325182(26)	1.628242(7)
120.00(1)	4.499634(10)	7.326634(26)	1.628273(7)
130.01(1)	4.500605(10)	7.328327(29)	1.628298(7)
140.00(2)	4.501701(10)	7.330170(29)	1.628311(7)
150.00(1)	4.502919(10)	7.332342(29)	1.628353(7)
160.00(1)	4.504265(10)	7.334608(29)	1.628370(7)
170.00(1)	4.505750(10)	7.337157(30)	1.628399(8)
180.01(0)	4.507390(11)	7.339809(32)	1.628394(8)
190.00(2)	4.509109(11)	7.342640(32)	1.628402(8)

200.00(1)	4.510969(11)	7.345651(33)	1.628398(8)
210.00(1)	4.512956(12)	7.348881(36)	1.628396(9)
220.00(1)	4.515025(13)	7.352359(37)	1.628420(9)
230.01(1)	4.517250(13)	7.355904(37)	1.628403(9)
240.01(1)	4.519561(13)	7.359533(38)	1.628373(10)
250.01(1)	4.521996(14)	7.363368(40)	1.628345(10)
240.00(1)	4.519563(13)	7.359479(38)	1.628361(10)
230.00(1)	4.517232(13)	7.355777(37)	1.628381(9)
219.99(1)	4.515044(12)	7.352214(36)	1.628381(9)
210.00(1)	4.512934(13)	7.348891(36)	1.628406(9)
200.00(1)	4.510942(12)	7.345628(34)	1.628402(9)
190.00(1)	4.509124(12)	7.342620(35)	1.628392(9)
180.00(1)	4.507343(11)	7.339763(32)	1.628401(8)
169.99(1)	4.505716(11)	7.337057(31)	1.628389(8)
160.00(1)	4.504226(11)	7.334582(31)	1.628378(8)
150.00(1)	4.502885(11)	7.332214(30)	1.628337(8)
140.00(1)	4.501644(10)	7.330155(29)	1.628328(7)
130.00(1)	4.500551(10)	7.328222(28)	1.628294(7)
120.00(2)	4.499623(10)	7.326375(27)	1.628220(7)
109.99(2)	4.498803(10)	7.324973(26)	1.628205(7)
99.99(3)	4.498123(10)	7.323853(26)	1.628202(7)
79.99(3)	4.497226(9)	7.322398(25)	1.628203(6)
59.98(3)	4.496933(9)	7.321901(24)	1.628199(6)
40.00(3)	4.497140(9)	7.322317(24)	1.628216(6)
20.00(2)	4.497507(9)	7.322958(23)	1.628226(6)
10.00(3)	4.497593(7)	7.323126(19)	1.628232(5)

Series 3 (Ice warmed to 170 K and cooled at 15 K min^{-1})

T (K)	*a*-axis (Å)	*c*-axis (Å)	*c*/*a* ratio
170.01(6)	4.506146(12)	7.337701(34)	1.628376(9)
10.00(2)	4.497551(7)	7.323407(18)	1.628310(5)
15.00(2)	4.497524(9)	7.323379(23)	1.628313(6)
19.99(2)	4.497471(9)	7.323300(23)	1.628315(6)
25.00(3)	4.497392(8)	7.323124(23)	1.628305(6)
30.00(3)	4.497279(9)	7.322963(23)	1.628310(6)
34.99(2)	4.497181(9)	7.322805(24)	1.628310(6)
40.00(4)	4.497107(9)	7.322626(23)	1.628297(6)
45.01(2)	4.497014(9)	7.322487(24)	1.628300(6)
50.01(3)	4.496941(9)	7.322398(24)	1.628306(6)
55.01(3)	4.496905(9)	7.322256(24)	1.628288(6)
60.00(3)	4.496902(9)	7.322203(25)	1.628277(6)
65.01(4)	4.496922(10)	7.322206(26)	1.628271(7)
70.01(3)	4.496969(9)	7.322285(24)	1.628271(6)

75.00(4)	4.497058(9)	7.322491(25)	1.628285(6)
79.99(3)	4.497177(9)	7.322667(25)	1.628281(6)
84.99(3)	4.497357(9)	7.322949(25)	1.628278(6)
90.00(1)	4.497565(9)	7.323245(26)	1.628269(7)
95.00(1)	4.497809(10)	7.323631(26)	1.628266(7)
100.00(1)	4.498090(10)	7.324071(26)	1.628262(7)
105.00(1)	4.498411(10)	7.324543(27)	1.628251(7)
110.00(1)	4.498782(10)	7.325027(27)	1.628224(7)
115.01(1)	4.499218(10)	7.325639(27)	1.628203(7)
120.00(1)	4.499621(10)	7.326415(29)	1.628229(7)
125.01(1)	4.500095(11)	7.327222(30)	1.628237(8)
130.01(1)	4.500576(10)	7.328137(29)	1.628266(7)
135.00(1)	4.501083(11)	7.329108(31)	1.628299(8)
140.00(1)	4.501642(11)	7.330134(29)	1.628325(8)
145.00(1)	4.502235(11)	7.331114(29)	1.628328(8)
150.00(1)	4.502856(11)	7.332276(30)	1.628361(8)
155.00(1)	4.503544(11)	7.333416(30)	1.628366(8)
160.00(1)	4.504247(11)	7.334546(30)	1.628362(8)
170.00(1)	4.505708(11)	7.337052(32)	1.628390(8)
180.01(0)	4.507320(11)	7.339752(32)	1.628407(8)
190.00(1)	4.509081(12)	7.342551(34)	1.628392(9)
200.01(1)	4.510931(12)	7.345648(33)	1.628411(9)
210.00(1)	4.512907(12)	7.348823(34)	1.628401(9)
220.00(1)	4.515018(12)	7.352220(35)	1.628392(9)
230.00(1)	4.517230(13)	7.355753(37)	1.628377(9)
240.01(1)	4.519569(14)	7.359488(39)	1.628361(10)
250.01(1)	4.521977(14)	7.363389(40)	1.628356(10)
260.01(1)	4.524534(14)	7.367392(40)	1.628321(10)
270.01(1)	4.527212(11)	7.371622(33)	1.628292(8)

Series 4 (Flash frozen D_2O globule)

T (K)	*a*-axis (Å)	*c*-axis (Å)	*c*/*a* ratio
9.99(3)	4.497540(8)	7.323524(21)	1.628340(5)
20.00(3)	4.497474(9)	7.323407(24)	1.628338(6)
30.00(3)	4.497291(9)	7.323134(24)	1.628343(6)
39.99(3)	4.497096(10)	7.322797(25)	1.628339(7)
50.00(3)	4.496942(9)	7.322484(25)	1.628325(6)
60.00(2)	4.496879(10)	7.322349(26)	1.628318(7)
70.00(1)	4.496945(10)	7.322481(25)	1.628323(7)
75.00(2)	4.497047(10)	7.322581(26)	1.628309(7)
80.00(1)	4.497181(10)	7.322754(26)	1.628299(7)
85.00(1)	4.497342(10)	7.322976(27)	1.628290(7)
90.00(1)	4.497553(10)	7.323335(26)	1.628293(7)
95.00(1)	4.497815(10)	7.323602(26)	1.628258(7)

100.00(1)	4.498125(10)	7.324005(26)	1.628235(7)
105.00(1)	4.498418(11)	7.324532(28)	1.628246(7)
110.00(1)	4.498778(11)	7.325138(28)	1.628251(7)
115.00(1)	4.499170(11)	7.325819(28)	1.628260(7)
120.00(1)	4.499596(11)	7.326530(29)	1.628264(8)
125.01(1)	4.500047(11)	7.327298(28)	1.628271(7)
130.01(1)	4.500551(12)	7.328145(30)	1.628277(8)
135.01(1)	4.501080(11)	7.329075(30)	1.628293(8)
140.01(1)	4.501640(11)	7.330070(30)	1.628311(8)
145.01(1)	4.502239(12)	7.331111(30)	1.628326(8)
150.01(1)	4.502863(12)	7.332233(32)	1.628349(8)
155.00(1)	4.503526(11)	7.333333(30)	1.628354(8)
160.00(1)	4.504221(12)	7.334540(31)	1.628370(8)
170.00(1)	4.505713(12)	7.337105(32)	1.628400(8)
180.00(1)	4.507348(12)	7.339719(32)	1.628390(8)
190.01(1)	4.509095(12)	7.342600(32)	1.628398(8)
200.00(1)	4.510942(13)	7.345660(34)	1.628409(9)
210.01(2)	4.512963(13)	7.348841(37)	1.628385(9)
220.00(1)	4.515051(13)	7.352252(36)	1.628387(9)
230.00(1)	4.517266(13)	7.355794(36)	1.628373(9)
240.01(1)	4.519610(14)	7.359577(39)	1.628366(10)
250.01(1)	4.522040(14)	7.363491(37)	1.628356(10)
260.00(1)	4.524590(15)	7.367566(40)	1.628339(10)
270.01(1)	4.527267(16)	7.371748(45)	1.628300(11)

Series 5 (Flash frozen D_2O droplet)

T (K)	*a*-axis (Å)	*c*-axis (Å)	*c*/*a* ratio
9.99(3)	4.497443(7)	7.323987(17)	1.628478(5)
20.00(3)	4.497348(9)	7.323858(23)	1.628484(6)
30.01(4)	4.497182(9)	7.323533(24)	1.628472(6)
40.00(4)	4.496997(9)	7.323247(24)	1.628475(6)
50.01(3)	4.496826(10)	7.322956(25)	1.628472(7)
60.00(3)	4.496792(9)	7.322798(24)	1.628449(6)
70.01(3)	4.496865(10)	7.322883(25)	1.628442(7)
80.00(3)	4.497088(10)	7.323181(27)	1.628427(7)
90.00(1)	4.497476(10)	7.323749(27)	1.628413(7)
100.00(1)	4.498002(10)	7.324630(27)	1.628419(7)
110.01(1)	4.498709(10)	7.325554(27)	1.628368(7)
120.00(1)	4.499577(12)	7.326591(32)	1.628284(8)
130.01(1)	4.500546(11)	7.328178(29)	1.628286(8)
140.00(1)	4.501663(11)	7.330067(30)	1.628302(8)
150.01(1)	4.502846(12)	7.332240(31)	1.628357(8)
160.00(1)	4.504230(12)	7.334548(33)	1.628369(9)
170.00(1)	4.505709(13)	7.337081(34)	1.628397(9)

180.01(1)	4.507341(12)	7.339767(33)	1.628403(9)
190.01(1)	4.509079(13)	7.342655(34)	1.628416(9)
200.00(1)	4.510922(13)	7.345695(37)	1.628424(9)
210.00(1)	4.512921(13)	7.348836(36)	1.628399(9)
220.00(1)	4.515021(13)	7.352251(38)	1.628398(10)
230.01(1)	4.517223(13)	7.355812(36)	1.628392(9)
240.00(1)	4.519558(13)	7.359517(36)	1.628371(9)
250.01(1)	4.522012(14)	7.363430(37)	1.628353(10)
260.00(1)	4.524569(15)	7.367425(41)	1.628315(11)

Series 6 (Slowly warmed KOD-doped ice with anneal at 70 K)

T (K)	*a*-axis (Å)	*c*-axis (Å)	*c*/*a* ratio
1.84(5)	4.497813(7)	7.319160(19)	1.627271(9)
4.99(1)	4.497821(9)	7.319192(24)	1.627275(13)
10.08(1)	4.497809(9)	7.319133(23)	1.627266(12)
14.97(3)	4.497781(9)	7.319114(23)	1.627272(12)
19.94(1)	4.497777(10)	7.319087(24)	1.627268(13)
24.76(1)	4.497712(10)	7.318954(24)	1.627262(13)
30.08(6)	4.497620(9)	7.318781(23)	1.627256(12)
35.19(1)	4.497503(9)	7.318630(24)	1.627265(13)
40.08(1)	4.497415(9)	7.318400(24)	1.627246(13)
45.00(1)	4.497334(9)	7.318289(24)	1.627250(13)
50.12(1)	4.497284(10)	7.318118(24)	1.627231(13)
55.24(1)	4.497248(10)	7.317956(26)	1.627208(14)
60.17(1)	4.497277(10)	7.317647(26)	1.627128(14)
65.21(1)	4.497333(10)	7.317556(26)	1.627088(14)
70.00(1)	4.497388(15)	7.317151(39)	1.626978(20)
80.00(1)	4.497238(11)	7.320335(29)	1.627740(15)
90.01(1)	4.497482(11)	7.321729(28)	1.627962(15)
100.01(1)	4.497957(11)	7.323074(29)	1.628089(15)
110.00(1)	4.498605(12)	7.324560(30)	1.628185(16)
120.01(1)	4.499408(11)	7.326199(30)	1.628258(16)
130.00(1)	4.500384(12)	7.327915(31)	1.628287(16)
140.00(2)	4.501472(12)	7.329884(31)	1.628330(16)
150.00(3)	4.502710(12)	7.332078(33)	1.628370(17)
160.01(1)	4.504116(12)	7.334342(33)	1.628364(17)
170.00(1)	4.505632(13)	7.336957(34)	1.628397(18)
180.00(1)	4.507294(13)	7.339676(35)	1.628400(18)
190.01(1)	4.509017(14)	7.342603(36)	1.628427(19)
200.00(1)	4.510927(14)	7.345639(37)	1.628410(19)
210.00(2)	4.512947(14)	7.348866(38)	1.628396(20)
220.00(1)	4.515059(14)	7.352415(39)	1.628421(20)

230.01(2)	4.517354(15)	7.355896(41)	1.628364(21)
240.00(2)	4.519708(16)	7.359623(45)	1.628340(23)
250.01(1)	4.522182(17)	7.363607(47)	1.628331(24)
260.00(2)	4.524754(19)	7.367703(51)	1.628310(26)
270.00(1)	4.527396(24)	7.371922(63)	1.628292(33)

Series 7 (Slowly cooled / warmed KOD-doped ice)

T (K)	*a*-axis (Å)	*c*-axis (Å)	*c*/*a* ratio
265.00(3)	4.525950(24)	7.369694(66)	1.628320(34)
255.00(1)	4.523293(22)	7.365499(58)	1.628349(30)
244.99(2)	4.520751(20)	7.361325(52)	1.628341(27)
235.00(1)	4.518391(18)	7.357548(48)	1.628356(25)
225.00(1)	4.516061(18)	7.353823(47)	1.628371(25)
215.00(1)	4.513867(17)	7.350299(44)	1.628382(23)
205.00(1)	4.511825(16)	7.346937(44)	1.628374(23)
195.00(1)	4.509871(16)	7.343777(40)	1.628379(21)
184.99(1)	4.508049(15)	7.340900(39)	1.628398(20)
174.99(1)	4.506337(15)	7.337946(40)	1.628362(21)
165.00(1)	4.504775(14)	7.335363(36)	1.628353(19)
155.00(1)	4.503253(13)	7.332884(34)	1.628353(18)
144.99(1)	4.501885(13)	7.330589(33)	1.628338(17)
134.99(2)	4.500772(12)	7.328660(32)	1.628312(17)
125.00(1)	4.499751(12)	7.326837(32)	1.628276(17)
114.99(1)	4.498870(12)	7.325110(32)	1.628211(17)
104.99(1)	4.498193(12)	7.323595(31)	1.628119(16)
94.99(1)	4.497611(11)	7.322309(29)	1.628044(15)
84.99(1)	4.497238(11)	7.321014(29)	1.627891(15)
75.00(2)	4.497072(11)	7.319615(28)	1.627640(15)
64.99(2)	4.497106(11)	7.318288(29)	1.627333(15)
54.98(2)	4.497106(11)	7.318096(28)	1.627290(15)
45.00(2)	4.497201(11)	7.318306(28)	1.627302(15)
35.00(2)	4.497386(11)	7.318646(27)	1.627311(14)
25.03(4)	4.497572(10)	7.318962(27)	1.627314(14)
15.01(2)	4.497693(11)	7.319166(26)	1.627316(14)
5.00(2)	4.497707(11)	7.319215(28)	1.627321(15)
10.02(4)	4.497706(10)	7.319221(26)	1.627323(14)
20.00(2)	4.497645(10)	7.319094(26)	1.627317(14)
29.99(3)	4.497486(11)	7.318778(29)	1.627304(15)
39.99(2)	4.497293(11)	7.318434(27)	1.627298(14)
50.00(1)	4.497132(11)	7.318176(27)	1.627298(14)
60.00(1)	4.497116(11)	7.317911(28)	1.627245(15)
70.00(1)	4.497123(11)	7.318563(28)	1.627388(15)
80.00(1)	4.497129(11)	7.320371(29)	1.627788(15)

90.01(1)	4.497444(11)	7.321641(28)	1.627956(15)
100.00(1)	4.497889(11)	7.322983(29)	1.628093(15)
110.01(1)	4.498539(11)	7.324442(30)	1.628182(16)
120.01(1)	4.499334(12)	7.326024(30)	1.628246(16)
130.00(1)	4.500333(12)	7.327808(32)	1.628281(17)
140.00(1)	4.501419(12)	7.329784(32)	1.628327(17)
150.00(1)	4.502687(13)	7.331942(33)	1.628348(17)
160.01(1)	4.504088(14)	7.334249(36)	1.628354(19)
170.00(1)	4.505622(14)	7.336852(37)	1.628377(19)
180.00(1)	4.507244(15)	7.339604(38)	1.628402(20)
190.01(1)	4.509048(15)	7.342498(39)	1.628392(20)
200.00(1)	4.510901(15)	7.345543(39)	1.628398(20)
210.00(2)	4.512918(15)	7.348736(39)	1.628378(20)
220.00(1)	4.515020(16)	7.352149(42)	1.628376(22)
230.01(2)	4.517287(17)	7.355804(44)	1.628368(23)
240.00(1)	4.519639(17)	7.359545(47)	1.628348(24)

Table S2: Calculated linear and volume thermal expansion coefficients as a function of temperature.

Series 1 (Naturally-frozen ice slow-cooled from 240 K)			
T (K)	α_a (x10^6 K^{-1})	α_c (x10^6 K^{-1})	α_V (x10^6 K^{-1})
230	50.4(7)	49.1(5)	149.9(9)
220	47.9(9)	47.3(7)	143.2(11)
210	45.4(9)	45.3(6)	136.1(11)
200	42.4(8)	42.8(6)	127.6(10)
190	39.8(8)	40.2(6)	119.8(10)
180	37.5(8)	37.7(5)	112.6(9)
170	34.5(8)	36.1(5)	105.0(9)
160	31.8(8)	33.0(5)	96.5(9)
150	29.2(7)	29.9(5)	88.3(9)
140	25.7(7)	27.8(5)	79.2(9)
130	22.0(7)	25.5(5)	69.5(9)
120	19.5(7)	22.0(5)	61.0(8)
110	16.7(7)	17.5(5)	50.9(8)
100	13.2(7)	13.5(5)	40.0(8)
90	10.0(7)	9.7(5)	29.7(8)
80	6.5(6)	6.1(5)	19.1(8)
70	3.2(6)	2.4(4)	8.9(7)
60	0.4(6)	−0.2(4)	0.5(7)
50	−2.2(6)	−2.0(4)	−6.4(7)
40	−3.8(6)	−4.4(4)	−12.1(7)
30	−4.2(6)	−5.0(4)	−13.3(7)
20	−2.9(5)	−2.7(4)	−8.4(7)
25	−3.8(6)	−3.7(4)	−11.2(7)
35	−4.2(6)	−4.2(4)	−12.6(7)
45	−3.1(6)	−3.6(4)	−9.8(7)
55	−1.1(6)	−1.7(4)	−3.8(7)
65	1.7(6)	1.2(4)	4.6(7)
75	4.9(6)	4.4(4)	14.2(7)
85	8.4(6)	7.8(4)	24.6(7)
95	11.9(6)	11.4(4)	35.2(8)
105	15.1(6)	15.1(4)	45.3(8)
115	17.9(6)	19.8(4)	55.7(8)
125	20.9(7)	24.0(5)	65.8(8)
135	24.3(7)	27.1(5)	75.6(9)
145	27.2(7)	29.0(5)	83.4(8)
155	30.0(8)	31.4(5)	91.4(9)
165	33.0(7)	34.6(5)	100.7(9)

175	36.1(8)	36.7(5)	108.9(10)
185	38.8(7)	38.9(5)	116.6(9)
195	41.5(8)	41.3(6)	124.4(10)
205	44.1(8)	43.7(6)	131.9(10)
215	46.3(8)	46.3(6)	138.9(10)
225	48.7(9)	48.3(6)	145.8(11)
235	51.4(9)	50.6(6)	153.5(11)
245	53.7(9)	52.9(7)	160.3(11)
255	56.2(9)	54.8(6)	167.3(11)

Series 2 (Naturally-frozen ice quenched from 265 to 77 K)

T (K)	α_a (x10^6 K^{-1})	α_c (x10^6 K^{-1})	α_V (x10^6 K^{-1})
20	−3.3(5)	−3.6(3)	−10.2(6)
30	−4.3(6)	−4.3(4)	−12.8(7)
40	−3.9(6)	−4.1(4)	−11.9(7)
50	−2.2(6)	−2.8(4)	−7.2(8)
60	0.1(6)	0.2(4)	0.4(8)
70	3.2(6)	3.5(4)	9.9(8)
80	6.5(6)	6.4(5)	19.4(8)
90	10.1(6)	9.4(4)	29.5(8)
100	14.1(6)	11.3(4)	39.5(8)
110	17.0(7)	15.9(5)	49.9(8)
120	19.7(7)	21.5(5)	60.9(8)
130	23.0(7)	24.1(5)	70.1(8)
140	25.7(7)	27.4(5)	78.8(9)
150	28.5(7)	30.3(5)	87.2(9)
160	31.4(7)	32.8(5)	95.7(9)
170	34.7(7)	35.5(5)	104.8(9)
180	37.3(7)	37.4(5)	111.9(9)
190	39.7(8)	39.8(6)	119.2(10)
200	42.7(8)	42.5(6)	127.8(10)
210	45.0(8)	45.7(6)	135.6(10)
220	47.6(9)	47.8(6)	142.9(11)
230	50.2(9)	48.8(7)	149.3(11)
240	52.5(9)	50.7(7)	155.8(11)
230	50.0(9)	49.4(7)	149.3(11)
220	47.6(9)	46.8(8)	142.0(11)
210	45.4(9)	44.8(6)	135.6(11)
200	42.2(9)	42.7(6)	127.1(11)
190	39.9(8)	39.9(6)	119.7(10)
180	37.8(8)	37.9(6)	113.5(10)
170	34.6(8)	35.3(6)	104.4(10)

160	31.4(8)	33.0(6)	95.8(9)
150	28.7(8)	30.2(6)	87.5(9)
140	25.9(7)	27.2(6)	79.1(9)
130	22.4(7)	25.8(6)	70.7(9)
120	19.4(7)	22.2(6)	61.0(8)
110	16.7(7)	17.2(6)	50.5(8)
95	11.7(4)	11.7(3)	35.1(5)
80	6.6(3)	6.7(2)	19.9(4)
60	0.5(3)	0.3(2)	1.2(4)
40	−3.2(3)	−3.6(2)	−10.0(4)
25	−3.4(4)	−3.7(3)	−10.4(5)

Series 3 (Ice warmed to 170 K and cooled at 15 K min^{-1})

T (K)	α_a (x10^6 K^{-1})	α_c (x10^6 K^{-1})	α_V (x10^6 K^{-1})
15	−1.8(10)	−1.5(7)	−5.0(12)
20	−2.9(12)	−3.5(8)	−9.4(14)
25	−4.3(12)	−4.6(8)	−13.1(15)
30	−4.7(12)	−4.4(8)	−13.7(14)
35	−3.8(12)	−4.6(8)	−12.3(15)
40	−3.7(12)	−4.3(9)	−11.8(15)
45	−3.7(12)	−3.1(9)	−10.5(15)
50	−2.4(12)	−3.2(9)	−8.0(15)
55	−0.9(12)	−2.7(9)	−4.4(15)
60	0.4(13)	−0.7(9)	0.1(15)
65	1.5(12)	1.1(9)	4.1(15)
70	3.0(13)	3.9(9)	9.9(16)
75	4.6(12)	5.2(9)	14.5(15)
80	6.6(13)	6.3(9)	19.6(15)
85	8.6(13)	7.9(9)	25.1(15)
90	10.1(13)	9.3(9)	29.4(16)
95	11.7(13)	11.3(9)	34.6(16)
100	13.4(13)	12.5(10)	39.2(17)
105	15.4(13)	13.1(10)	43.8(17)
110	17.9(14)	15.0(10)	50.8(17)
115	18.6(14)	18.9(10)	56.2(17)
120	19.5(14)	21.6(10)	60.6(17)
125	21.2(14)	23.5(10)	66.0(18)
130	22.0(15)	25.7(11)	69.6(19)
135	23.7(15)	27.3(10)	74.6(18)
140	25.6(15)	27.4(11)	78.6(19)
145	27.0(15)	29.2(11)	83.2(18)
150	29.1(15)	31.4(11)	89.5(18)
155	30.9(15)	31.0(11)	92.7(19)
162.5	32.0(10)	33.1(7)	97.1(12)

170	34.1(8)	35.5(5)	103.7(9)
180	37.4(8)	37.5(6)	112.3(10)
190	40.1(8)	40.2(6)	120.3(10)
200	42.4(8)	42.7(6)	127.6(10)
210	45.3(8)	44.7(6)	135.3(10)
220	47.9(9)	47.2(6)	142.9(11)
230	50.4(9)	49.4(6)	150.2(11)
240	52.5(9)	51.9(7)	157.0(11)
250	54.9(10)	53.7(7)	163.6(12)
260	57.9(9)	55.9(7)	171.7(12)

Series 4 (Flash frozen D_2O globule)

T (K)	α_a (x10^6 K^{-1})	α_c (x10^6 K^{-1})	α_V (x10^6 K^{-1})
20	−2.8(6)	−2.7(4)	−8.2(7)
30	−4.2(6)	−4.2(4)	−12.6(8)
40	−3.9(6)	−4.4(4)	−12.2(8)
50	−2.4(7)	−3.1(5)	−7.9(8)
60	0.0(6)	0.0(4)	0.0(8)
67.5	2.5(9)	2.1(6)	7.1(11)
75	5.2(13)	3.7(9)	14.2(16)
80	6.6(13)	5.4(10)	18.5(17)
85	8.3(13)	7.9(9)	24.5(16)
90	10.5(14)	8.5(10)	29.6(17)
95	12.7(13)	9.1(9)	34.6(16)
100	13.4(14)	12.7(10)	39.5(17)
105	14.5(14)	15.5(10)	44.5(17)
110	16.7(15)	17.6(10)	51.0(18)
115	18.2(15)	19.0(10)	55.4(18)
120	19.5(15)	20.2(10)	59.2(18)
125	21.2(15)	22.0(11)	64.5(18)
130	23.0(15)	24.3(10)	70.2(18)
135	24.2(16)	26.3(11)	74.7(19)
140	25.7(15)	27.8(11)	79.3(19)
145	27.2(16)	29.5(11)	83.8(19)
150	28.6(16)	30.3(11)	87.5(19)
155	30.2(16)	31.5(11)	91.8(20)
162.5	32.4(10)	34.3(7)	99.0(13)
170	34.7(8)	35.3(6)	104.7(10)
180	37.5(8)	37.4(6)	112.5(10)
190	39.9(8)	40.5(6)	120.2(10)
200	42.9(8)	42.5(6)	128.3(10)
210	45.5(9)	44.9(6)	136.0(11)
220	47.7(9)	47.3(6)	142.7(11)

230	50.5(9)	49.8(6)	150.8(11)
240	52.8(9)	52.3(6)	158.0(11)
250	55.1(10)	54.3(7)	164.5(12)
260	57.8(10)	56.1(7)	171.7(12)

Series 5 (Flash frozen D_2O droplet)

T (K)	α_a (x10^6 K^{-1})	α_c (x10^6 K^{-1})	α_V (x10^6 K^{-1})
20	−2.9(5)	−3.1(3)	−8.9(6)
30	−3.9(6)	−4.2(4)	−12.0(7)
40	−4.0(6)	−3.9(4)	−11.9(8)
50	−2.3(6)	−3.1(4)	−7.6(7)
60	0.4(7)	−0.5(5)	0.4(8)
70	3.3(6)	2.6(4)	9.2(8)
80	6.8(7)	5.9(5)	19.5(8)
90	10.2(7)	9.9(5)	30.2(8)
100	13.7(7)	12.3(5)	39.7(8)
110	17.5(7)	13.4(5)	48.4(9)
120	20.4(7)	17.9(5)	58.7(9)
130	23.2(8)	23.7(6)	70.1(10)
140	25.6(8)	27.7(5)	78.8(9)
150	28.5(8)	30.6(5)	87.6(10)
160	31.8(8)	33.0(6)	96.6(10)
170	34.5(8)	35.6(6)	104.6(10)
180	37.4(9)	38.0(6)	112.8(11)
190	39.7(9)	40.4(6)	119.8(10)
200	42.6(9)	42.1(6)	127.3(11)
210	45.4(9)	44.6(7)	135.5(11)
220	47.7(9)	47.5(6)	142.8(11)
230	50.2(9)	49.4(7)	149.9(11)
240	53.0(9)	51.8(6)	157.8(11)
250	55.4(9)	53.7(7)	164.6(11)

Series 6 (Slowly warmed KOD-doped ice with anneal at 70 K)

T (K)	α_a (x10^6 K^{-1})	α_c (x10^6 K^{-1})	α_V (x10^6 K^{-1})
3.42	0.6(33)	1.4(23)	3(4)
7.54	−0.5(24)	−1.6(17)	−3(3)
12.52	−1.3(24)	−0.5(17)	−3(3)
17.45	−0.2(25)	−0.7(17)	−1(3)
22.35	−3.0(27)	−3.8(19)	−10(3)
27.42	−3.8(24)	−4.4(17)	−12(3)

32.64	−5.1(24)	−4.1(17)	−14(3)
37.64	−4.0(25)	−6.4(18)	−14(3)
42.54	−3.7(25)	−3.1(18)	−10(3)
47.56	−2.2(24)	−4.6(17)	−9(3)
52.68	−1.6(25)	−4.3(18)	−7(3)
57.71	1.3(27)	−8.6(19)	−6(3)
62.69	2.5(27)	−2.5(19)	2(3)
75	−3.3(19)	43.5(14)	36.8(23)
85	5.4(15)	19.0(10)	29.9(18)
95	10.6(15)	18.4(10)	39.5(18)
105	14.4(15)	20.3(11)	49.1(18)
115	17.8(16)	22.4(11)	58.0(19)
125	21.7(15)	23.4(11)	66.9(19)
135	24.2(16)	26.9(11)	75(2)
145	27.5(16)	30.0(11)	85(2)
155	31.2(17)	30.8(12)	93(2)
165	33.7(17)	35.7(12)	103(2)
175	36.9(18)	37.1(12)	111(2)
185	38.2(18)	39.8(13)	116(2)
195	42.4(19)	41.4(13)	126(2)
205	44.8(19)	43.9(13)	133(2)
215	47(2)	48.3(14)	142(2)
225	51(2)	47.3(14)	149(2)
235	52(2)	50.7(15)	155(3)
245	55(2)	54.1(16)	163(3)
255	57(2)	55.7(17)	170(3)
265	58(3)	57.3(19)	174(3)

Series 7 (Slowly cooled / warmed KOD-doped ice)

T (K)	α_a (x10^6 K^{-1})	α_c (x10^6 K^{-1})	α_V (x10^6 K^{-1})
260	59(3)	57(2)	174(4)
250	56(3)	57(2)	169(4)
240	52(3)	51.3(19)	156(3)
230	52(2)	50.6(17)	154(3)
220	49(2)	47.9(17)	145(3)
210	45(2)	45.7(16)	136(3)
200	43(2)	43.0(15)	130(3)
190	40(2)	39.1(15)	120(3)
180	38(2)	40.2(14)	116(2)
170	35(2)	35.2(14)	105(2)
160	33.8(18)	33.8(12)	101(2)
150	30.4(17)	31.3(12)	92(2)

140	24.7(17)	26.3(12)	76(2)
130	22.7(16)	24.9(12)	70(2)
120	19.6(16)	23.6(12)	63(2)
110	15.0(16)	20.7(11)	51(2)
100	12.9(16)	17.6(11)	43.4(19)
90	8.3(15)	17.7(11)	34.3(18)
80	3.7(15)	19.1(10)	26.5(18)
70	-0.8(15)	18.1(10)	16.6(18)
60	0.0(15)	2.6(10)	2.6(18)
50	−2.1(15)	−2.9(10)	−7.1(18)
40	−4.1(15)	−4.6(10)	−12.9(18)
30	−4.2(14)	−4.3(10)	−12.6(17)
20	−2.7(14)	−2.8(10)	−8.1(17)
10	−0.3(14)	−0.7(10)	−1.3(17)
15	−1.4(13)	−1.7(9)	−4.5(16)
25	−3.5(14)	−4.3(10)	−11.4(17)
35	−4.3(15)	−4.7(10)	−13.3(18)
45	−3.6(14)	−3.5(10)	−10.7(17)
55	−0.4(14)	−3.6(10)	−4.3(18)
65	0.2(15)	8.9(10)	9.2(18)
75	0.1(14)	24.7(10)	25.0(18)
85	7.0(15)	17.3(10)	31.3(18)
95	9.9(15)	18.3(10)	38.1(18)
105	14.4(15)	19.9(11)	48.8(18)
115	17.7(15)	21.6(11)	56.9(19)
125	22.2(16)	24.4(11)	68.8(19)
135	24.1(16)	27.0(12)	75(2)
145	28.2(17)	29.4(12)	86(2)
155	31.1(18)	31.4(12)	94(2)
165	34.1(19)	35.5(13)	104(2)
175	36.0(19)	37.5(13)	110(2)
185	40(2)	39.4(14)	119(2)
195	41(2)	41.5(14)	124(2)
205	45(2)	43.5(14)	133(2)
215	47(2)	46.4(14)	140(3)
225	50(2)	49.7(15)	150(3)
235	52(2)	50.1(16)	155(3)

Section S3. Parameterisation of the volume thermal expansion

A variety of physically meaningful functional forms may be used to fit the temperature variation of lattice parameters as a function of temperature. Following closely the example used in my previous work,[22] the volume thermal expansion is parameterised using a model in which the vibrational density of states (VDOS) is described by two Debye-type functions and an Einstein-type function. A more detailed justification for the application of this model is given in my earlier work.

The temperature dependence of the molar volume is thus described as

$$V = V_0 \left[1 + \frac{f(\theta_{D1})}{X} + \frac{f(\theta_{D2})}{Y} + \frac{f(\theta_E)}{Z} \right] \quad (1)$$

where V_0 is the molar volume at zero temperature, the Debye functions and the Einstein function, $f(\theta_{D1})$, $f(\theta_{D2})$ and $f(\theta_E)$, represent different components of the crystal's internal energy and X, Y and Z are 'mixing parameters'. Where the volume is described in terms of single Debye temperature in a first-order expansion of the internal energy the term X, for example, would be V_0K_0/γ, where V_0 and K_0 are the zero-temperature molar volume and bulk modulus and γ is a Grüneisen parameter. For the three-term model given in Eq. 1 it is sufficient to note that $X \propto \gamma_x^{-1}$, where γ_x is a Grüneisen parameter corresponding to the vibrational modes described by $f(\theta_{D1})$.

The Debye and Einstein functions are defined as

$$f(\theta_D) = 9Nk_BT\left(\frac{T}{\theta_D}\right)^3 \int_0^{\theta_D/T} \frac{x^3}{e^x - 1} dx \quad (2)$$

$$f(\theta_E) = 3Nk_B\left(\frac{\theta_E}{e^{\theta_E/T} - 1}\right) \quad (3)$$

where N is the number of atoms per molecules, k_B is Boltzmann's constant, T = temperature, and θ_D and θ_E are characteristic Debye or Einstein temperatures, respectively, corresponding to the cut-off frequencies of particular vibrational modes in the VDOS.

It was clear by visual inspection that the volume thermal expansion in D_2O ice obtained by slow cooling, and subjected to various thermal protocols, does not differ substantially from that of flash-frozen ice. A fit of the double-Debye + Einstein model using the same cut-off frequencies as were reported previously (Table S3, column 1) produced a satisfactory fit to the Series 1A/1B data with only small adjustments to the mixing parameter values (Table S3, column 2). In fact the difference in the X parameter can be attributed to poor sampling of the lattice-parameter saturation below 10 K in this study. Free refinement of all parameters (Table S3, column 3) yields a small improvement in the quality of the fit.

Table S3: Parameters obtained by fitting of a model constructed from a double-Debye + Einstein-type function (Eqs. 1 – 3).

		Quenched D_2O ice Fortes[22] Series 1 & 2	Naturally-frozen ice This work, Series 1 Frequencies fixed	Naturally-frozen ice This work, Series 1 All parameters free
V_0	($cm^3\ mol^{-1}$)	19.31434 ± 0.00006	19.31418 ± 0.00011	19.31401 ± 0.00022
V_0	($Å^3$)	128.2889 ± 0.0004	128.2878 ± 0.0007	128.2867 ± 0.00011
θ_{D1}	(K)	88.9 ± 6.6	*88.9*	87.4 ± 9.8
θ_{D2}	(K)	476.9 ± 18.9	*476.9*	477 ± 20
θ_E	(K)	937 ± 43	*937*	938 ± 42
X	($J\ mol^{-1}$)	$-317 \pm 24\ x10^4$	$-299.1 \pm 2.4\ x10^4$	$-307 \pm 30\ x10^4$
Y	($J\ mol^{-1}$)	$48.6 \pm 2.2\ x10^4$	$47.0 \pm 0.2\ x10^4$	$47 \pm 2\ x10^4$
Z	($J\ mol^{-1}$)	$42.2 \pm 1.1\ x10^4$	$47.1 \pm 0.4\ x10^4$	$46 \pm 1\ x10^4$
Residual sum of sq.		$3.167\ x10^{-4}$	$3.277\ x10^{-6}$	$2.714\ x10^{-6}$

A discussion of the physical meaning of these parameters is given by Fortes.[22] The volume thermal expansion calculated from this model fit is shown below with the raw derivatives from the current study of pure ice in Figure S1a, from the previous work in Figure S1b and with this work's KOD-doped ice data in Figure S1c. It is apparent that the scatter in the data from the earlier work is larger (by a factor of ~ 2) than in the current work. The standard deviation of the model residuals are $2.2\ x10^{-6}$ for the three data series measured in 2017 and $9.8\ x10^{-7}$ for the seven data series measured in 2018. This is almost certainly due to the extra care afforded to ensure good thermal equilibration of the sample at each temperature point, equilibration time being increased from 5 minutes to 10 minutes. There is a small but clear deviation from the model fit in the region between 100 and 150 K and above 230 K, which probably reflects the lack of any description in the model of the effect on the VDOS of partial ordering ± any structural relaxation as well as poor sampling of the higher frequency portion of the VDOS.

Figure S1.

(a) Volume thermal expansion data and model fit (solid black line) from the current work. The dashed blue line is taken from the capacitance dilatometry study of single-crystal D_2O ice by Buckingham.[23] The general deviation that grows with temperature may reflect poor thermal equilibrium of the crystal with its surroundings whilst the larger deviation at high temperatures may be due to incomplete correction for the effects of sample sublimation.
(b) Volume thermal expansion data from the previous work[22] compared with the model fit (solid black line) from the current work. **(c)** Volume thermal expansion of KOD-doped D_2O ice I*h* compared with the model fit (solid black line) from the analysis of pure D_2O ice.

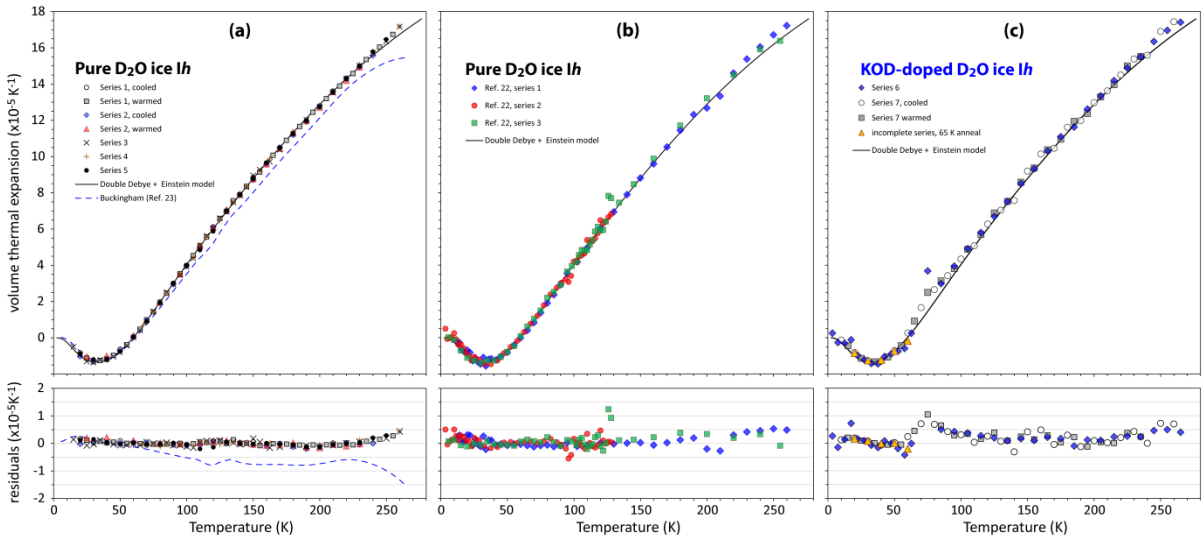

There is little change in the temperature at which the volume thermal expansion turns negative, 59.75 K (59.9 K in the previous work) or the temperature of the negative expansion minimum, 32.0 K (32.6 K previously). Despite small anomalies in α_V between 100 and 150 K, the level of reproducibility of this quantity, across ten different temperature series on six independently-prepared and loaded specimens measured over two years is very good. Clearly, this description of the thermal expansion is sufficiently robust for most ordinary purposes; for example, applications in modelling of icy planetary bodies.

Section S4. Analytical description of the *c*/*a* ratio temperature dependence

The objective is to present an analytical approximation to the temperature dependence of the *c*/*a* ratio in ice I*h* and use that to calculate the effect on the *c*-axis linear expansion of freezing-in non-equilibrium values of the axial ratio and allowing that quantity to either merge smoothly with the equilibrium value or to undergo a sharp relaxation. The underlying assumption of this model is that features in *c*/*a* are entirely due to the behaviour of the *c*-axis. This is, of course, not entirely true since there is a small lattice-parameter dispersion in the *a*-axis at low temperature, but it is approximately three times smaller than the relative dispersion in the *c*-axis length. It is nevertheless self-evident from the calculations below that this simple model gives an accurate representation of the thermal expansion anomalies and aids in understanding their origin where absolute lattice parameters (and thus absolute *c*/*a* ratios) may be unavailable, such as in dilatometry studies.

The linear expansion of the *c*-axis, $\alpha_c = \frac{1}{c}\frac{dc}{dT}$

where the temperature dependence of the *c*-axis length, $c(T) = a(T) \cdot (c/a)(T)$

The temperature dependence of the *a*-axis length is obtained by approximating a three term Einstein model of the vibrational spectrum to experimental values:

$$a(T) = a_0 + \left[\frac{x}{exp(\theta_{E1}/T) - 1}\right] + \left[\frac{y}{exp(\theta_{E2}/T) - 1}\right] + \left[\frac{z}{exp(\theta_{E3}/T) - 1}\right]$$

These parameters have the following values:

a_0	4.4976				
x	−0.003	y	0.0230	z	0.1746
θ_{E1}	85	θ_{E2}	240	θ_{E3}	600

The temperature dependence of the axial ratio is approximated as:

$$(c/a)(T) = P(T) \cdot m(T) + (1 - P(T)) \cdot n(T) \cdot Q(T)$$

Both $m(T)$ and $n(T)$ are polynomial curves intended to represent the upper and lower bounds of the axial ratio's temperature dependence, with the smooth variation between them being described primarily by a Gompertz function, $P(T)$, with an additional logistic function, $Q(T)$ being employed to describe the shape of the discontinuity in the 100 – 130 K region.

$$m(T) = uT^3 + vT^2 + wT + (c/a)_{high}$$

$$n(T) = uT^3 + vT^2 + wT + (c/a)_{low}$$

u = 8.2 x 10^{-12}, v = 7.2 x10^{-9}, w = 3.3 x 10^{-8}, $(c/a)_{high}$ = 1.62865 and $(c/a)_{low}$ = 1.62825.

$$P(T) = a \cdot exp\left(-b \cdot exp\left(-c(T - T_1)\right)\right)$$

In all of the models described subsequently, except model Type 4, the parameters in this equation take the values, a = 1.1, b = 0.6, c = 0.035 and T_1 = 145 K; this is the solid black line in Figure 5 of the main text and supplementary figures S2 – S3, below. N.B., in this case $Q(T)$ = 1.

In order to demonstrate the effect of frozen-in c/a ratios and of the structural relaxations in the 100 – 130 K region, I use,

$$Q(T) = \frac{d + (e - d)}{1 + exp\big(f(T - T_2)\big)}$$

The parameters adopted for each of the curves used in various figures, both here and in the main text, are given below.

Model **Type 1**: Frozen-in c/a ratios with no relaxation. The coloured lines referred to are plotted in Figure 5a – 5c of the main text.

	d	e	f	T_2
Solid black line*	-	-	-	-
Dotted blue line	1.00000	1.00005	0.10	115
Dashed green line	1.00000	1.00010	0.07	124
Dashed orange line	1.00000	1.00015	0.06	135
Solid red line	0.99999	1.00025	0.05	170

* $Q(T)$ = 1

Model **Type 2**: Frozen-in c/a ratios with relaxation. The coloured lines referred to are plotted in Figure 5d – 5f of the main text.

	d	e	f	T_2
Dotted blue line	1.00000	1.00005	0.35	100
Dashed green line	1.00000	1.00010	0.25	105
Dashed orange line	1.00000	1.00015	0.20	110

Model **Type 3**: (a) Samples with the same degree of frozen-in c/a ratio but with varying degrees of relaxation. The coloured lines referred to are plotted in Supplementary Figure S2 below.

	d	e	f	T_2
Dotted blue line	1.00000	1.00010	0.35	100
Dashed green line	1.00000	1.00010	0.22	106
Dashed orange line	1.00000	1.00010	0.15	112

Model **Type 4**: (a) Hypothetical different variations in the overall temperature dependence of the *c*/*a* ratio. In all cases shown here, $Q(T) = 1$. The coloured lines referred to are plotted in Supplementary Figure S3 below.

	a	*b*	*c*	T_1
Solid black line	1.10	0.60	0.035	145
Dotted blue line	1.13	0.60	0.025	150
Dashed green line	1.16	0.65	0.018	152
Dashed orange line	1.10	1.00	0.050	133
Solid red line	1.10	1.00	0.080	135

Figure S2
(a) Hypothetical variations of the *c*/*a* ratio, following model Type 3; solid black and red lines are as shown in the Type 1 example (Fig. 5). **(b)** Calculated linear expansion along the *c*-axis for these scenarios; the feature marked (1) is similar to what was observed in my earlier study of H_2O ice I*h* (Ref. 22, Figures 9 and 12). **(c)** Enlarged view of the region where step-like anomalies in the linear expansion occur.

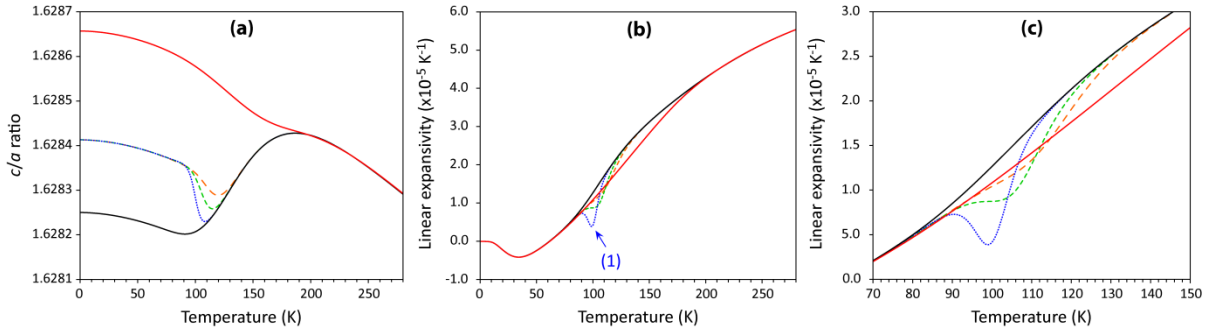

Figure S3
(a) Hypothetical variations of the *c*/*a* ratio, following model Type 4. **(b)** Calculated linear expansion along the *c*-axis for these scenarios. The very steep turn-over depicted by the red curve, which leads to the sharp rise followed by a plateau in α_c, is a reasonable approximation to the behaviour seen in KOD-doped ice (*cf.*, Fig. 4f).

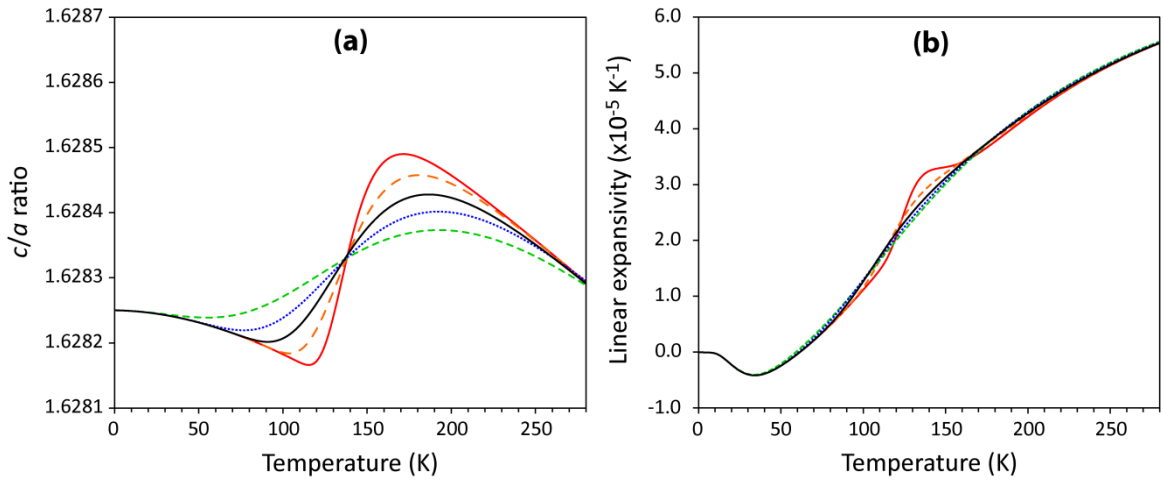

Section S5. Additional supplementary figures

Figure S4

Relaxation times in H_2O and D_2O ice as a function of T.[15,16,23,33,35,36,38-40] The bold dashed red lines bounding the spread of low-T data depict activation energies due to orientational defects (E_A = 59 kJ mol^{-1}, τ_0 = 1.50x10^{-16} s) and ionic defects (E_A = 20 kJ mol^{-1}, τ_0 = 2.20x10^{-8} s). Finer dotted lines show different values of the parameter 'p' (in black) proposed by Popov et al.[44] to characterise the resistance to defect migration from correlated movement of orientational and ionic defects. Higher values of p are indicative of greater influence on the relaxation time from orientational defects. The shaded region shows the range of temperatures over which relaxation times of 10^3 – 10^4 s may occur in ice by virtue of the sample-specific defect population.

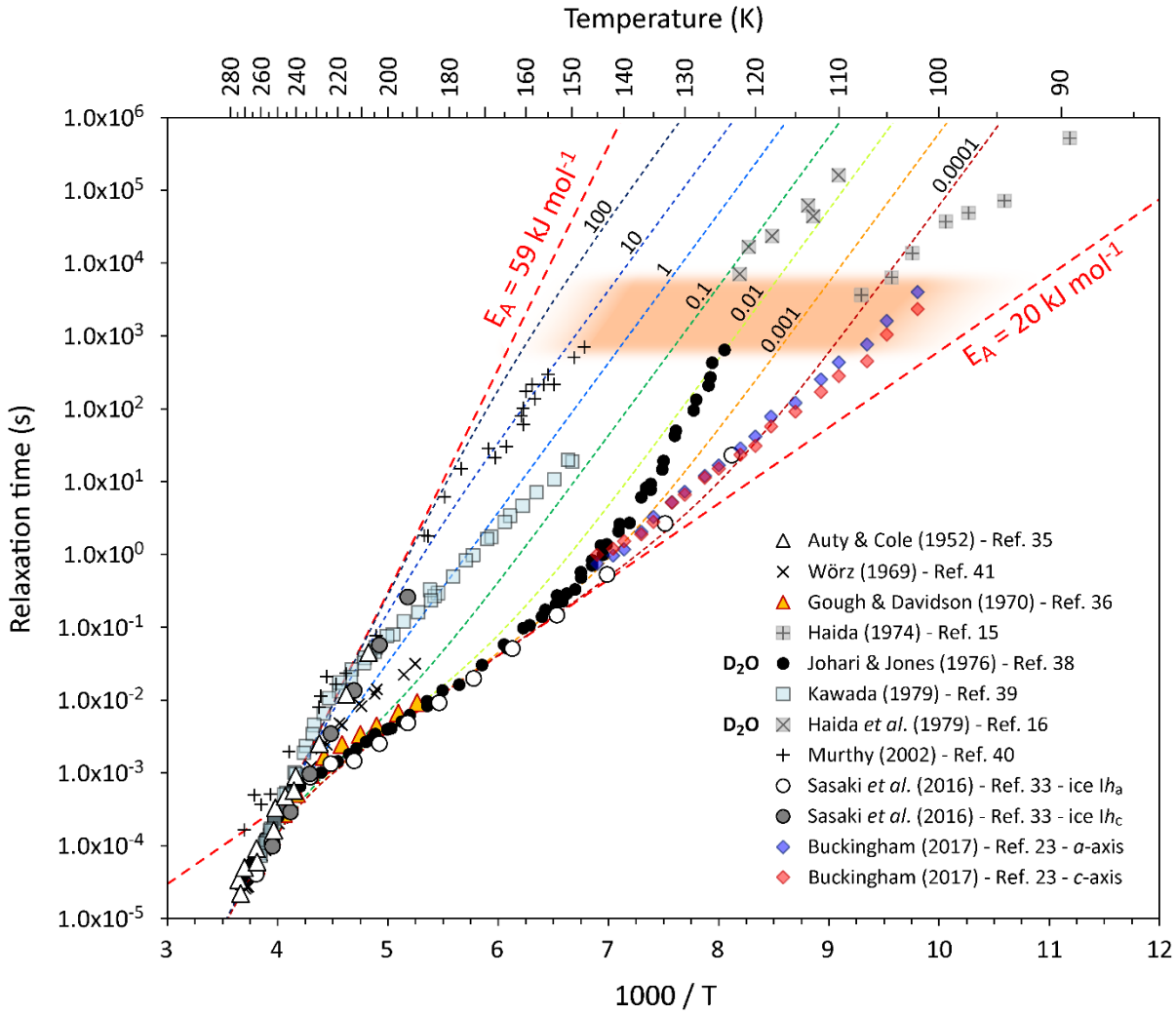

Figure S5

Neutron powder diffraction data measured in HRPD's 90° detector banks for a representative set of data collected at 10 K in the current study. In all cases, the lack of any diffuse scattering between the strong (011), (020) and (100) peaks is evidence, along with the near uniform sharpness of all peaks, that the samples are not significantly affected by stacking faults.

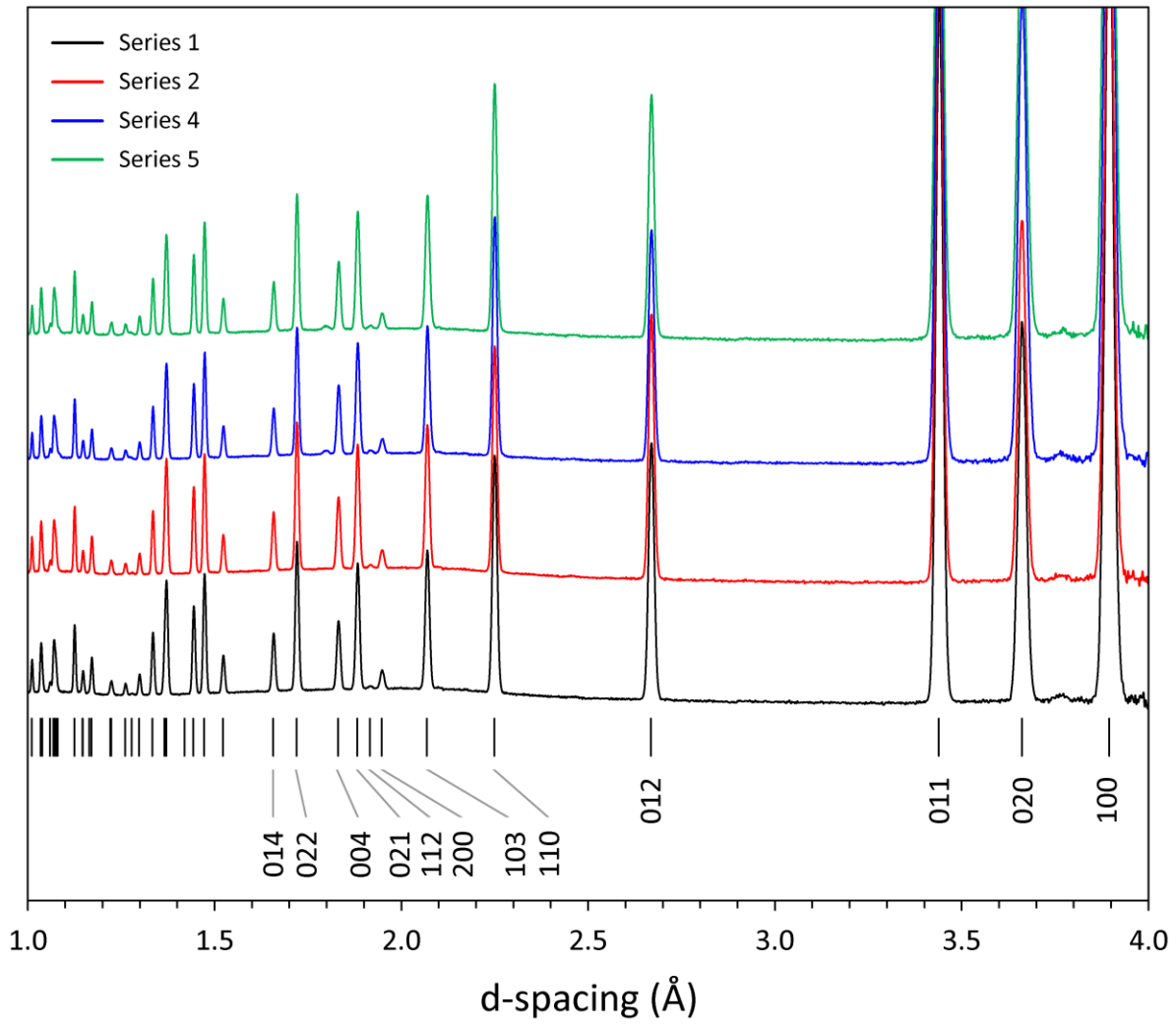

Figure S6

Variation of the full width at half maximum of the (002) and (011) Bragg peaks – measured in HRPD's 90° detector banks – as a function of temperature. **(a)** The naturally-frozen, slow-cool / slow warm observations (Series 1) exhibit no discernible variation in peak width with temperature. By contrast, the flash-frozen samples exhibit broadening of up to 8 % that do vary with temperature. **(b)** It is clearer from the plot of (011) peak widths that the onset of the sharpening in the flash frozen samples occurs at 150 K on warming, with each becoming as sharp or even sharper than the naturally-frozen ice specimens at higher homologous temperatures. It is noteworthy that, despite being synthesised in a similar way to the 2018 quenched pipette droplets, the 2017 quench samples exhibit a much smaller degree of peak broadening. It seems likely that other undocumented (and indeed unmeasurable) aspects of the sample preparation have a significant effect on the diffraction characteristics of the specimen. **(c)** and **(d)** Variation in peak widths obtained in Series 2, where the sample was quenched from 265 to 77 K in 90 seconds and then cooled to 10 K over the course of another hour. The grey background symbols depict the data shown in Figure S6a and S6b. Evidently, the rapid quenching and freezing-in of the high-temperature disorder (and high-temperature *c*/*a* ratio) does not result in any broadening due to inhomogeneous strain.

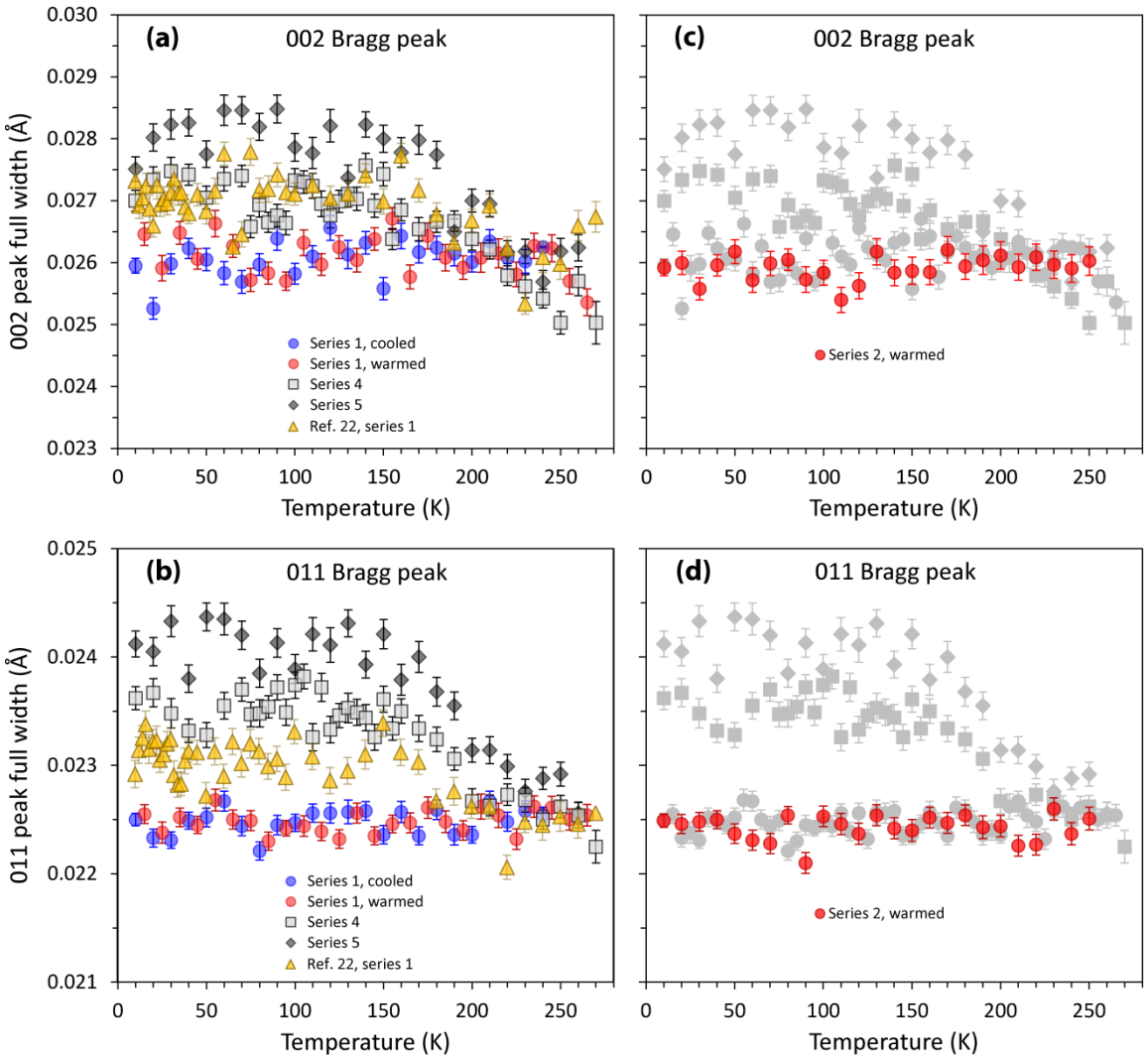

Figure S7.

(a) For context, the widths of the (002) peak shown in Figure S6 are compared with the widths observed in heavily stacking-faulted ice formed by the back-transformation of high-pressure ice VI. **(b)** Neutron powder data measured in HRPD's 90° detectors during the transition from ice VI→ ice I*h* via stacking-faulted ice I_{SD}, showing the large variations in peak width, intensity and diffuse background that occur during this transformation.

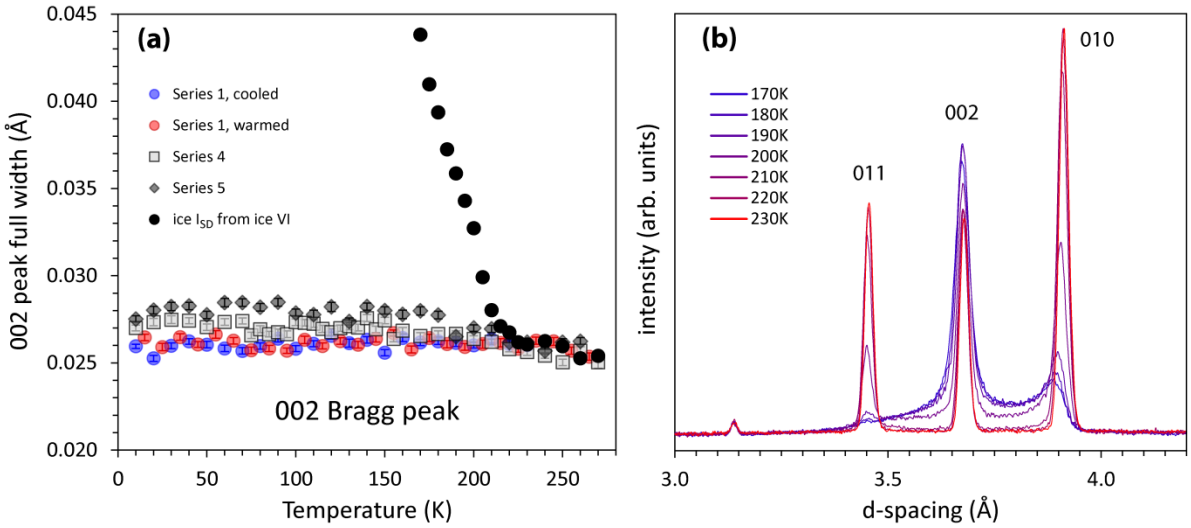

Section S6. References

Literature cited in this Supplement (complete numbered list in main text)

[22] A. D. Fortes, Accurate and precise lattice parameters of H_2O and D_2O ice I*h* between 1.6 and 270 K from high-resolution time-of-flight neutron powder diffraction data. *Acta Crystallogr. B* **74**, 196–216 (2018).

[23] D. T. W. Buckingham, High-resolution thermal expansion and dielectric relaxation measurements of H_2O and D_2O ice I*h*. PhD Thesis, Montana State University (2017).

[33] K. Sasaki, R. Kita, N. Shinyashiki, S. Yagihara, Dielectric relaxation time of ice-I*h* with different preparation. *J. Phys. Chem. B.*, **120**, 3950–3953 (2016).

[35] R. P. Auty, R. H. Cole, Dielectric properties of ice and solid D_2O. *J. Chem. Phys.*, **20**, 1309–1314 (1952).

[38] S. R. Gough, D. W. Davidson, Dielectric behavior of cubic and hexagonal ices at low temperatures. *J. Chem. Phys.*, **52**, 5442–5449 (1970).

[59] G. P. Johari, S. J. Jones, Dielectric properties of polycrystalline D_2O ice I*h* (hexagonal). *Proc. R. Soc. London A*, **349**, 467–495 (1976).

[39] S. Kawada, Dielectric properties of heavy ice I*h* (D_2O ice). *J. Phys. Soc. Japan*, **47**, 1850–1856 (1979).

[40] S. S. N. Murthy, Slow relaxation in ice and ice clathrates and its connection to the low-temperature phase transition induced by dopants. *Phase Trans.*, **75**, 487–506 (2002).

[41] O. Wörz, R. H. Cole, Dielectric properties of ice I. *J. Chem. Phys.*, **51**, 1546–1551 (1969).

[44] I. Popov, I. Lunev, A. Khamzin, A. Greenbaum, Y. Gusev, Y. Feldman, The low-temperature dynamic crossover in the dielectric relaxation of ice I*h*. *Phys. Chem. Chem. Phys.*, **19**, 28610–28620 (2017).